

Emissive and charge-generating donor-acceptor interfaces for organic optoelectronics with low voltage losses

Peer-reviewed author version

Ullbrich, Sascha; Benduhn, Johannes; Jia, Xiangkun; Nikolis, Vasileios C.; Tvingstedt, Kristofer; PIERSIMONI, Fortunato; Roland, Steffen; Liu, Yuan; Wu, Jinhan; Fischer, Axel; Neher, Dieter; Reineke, Sebastian; SPOLTORE, Donato & VANDEWAL, Koen (2019) Emissive and charge-generating donor-acceptor interfaces for organic optoelectronics with low voltage losses. In: Nature materials, 18 (5), p. 459-+.

DOI: 10.1038/s41563-019-0324-5

Handle: <http://hdl.handle.net/1942/30164>

Emissive and Charge-Generating Donor-Acceptor Interfaces for Organic Optoelectronics with Low Voltage Losses

Sascha Ullbrich^{1,#,*}, Johannes Benduhn^{1,#,*}, Xiangkun Jia^{1,#}, Vasileios C. Nikolis¹, Kristofer Tvingstedt², Fortunato Piersimoni³, Steffen Roland³, Yuan Liu¹, Jinhan Wu¹, Axel Fischer¹, Dieter Neher³, Sebastian Reineke¹, Donato Spoltore¹, Koen Vandewal^{1,‡,*}

* Corresponding authors (sascha.ullbrich@tu-dresden.de, johannes.benduhn@tu-dresden.de, koen.vandewal@uhasselt.be)

These authors contributed equally to the manuscript

¹ Dresden Integrated Center for Applied Physics and Photonic Materials (IAPP) and Institute for Applied Physics, Technische Universität Dresden, Nöthnitzer Str. 61, 01187 Dresden, Germany

² Experimental Physics VI, Julius-Maximilian University of Würzburg, 97074 Würzburg, Germany

³ Institute of Physics and Astronomy, University of Potsdam, Karl-Liebknecht-Str. 24-25, 14476 Potsdam, Germany

‡ Current address: Institute for Materials Research (IMO-IMOMEC), Hasselt University, Wetenschapspark 1, 3590 Diepenbeek, Belgium

Introductory Paragraph

Intermolecular charge-transfer (CT) states at the interface between electron donating (D) and accepting (A) materials are crucial for the operation of organic solar cells (OSCs) but can also be exploited for organic light-emitting diodes (OLEDs) [1] [2]. Non-radiative CT state decay is dominant in state-of-the-art D-A based OSCs, and is responsible for large voltage losses and relatively low power-conversion efficiencies (PCEs) as well as electroluminescence (EL) external quantum yields (EQE_{EL}) in the 0.01-0.0001% range [3] [4]. In contrast, EQE_{EL} reaches up to 16% in D-A based OLEDs [5] [6] [7]. Here, we show that proper control of CT state properties allows simultaneous occurrence of a high photovoltaic and emission quantum yield within a single, visible-light-emitting D-A system. This leads to ultra-low emission turn-on voltages as well as significantly reduced voltage losses upon solar illumination. These results unify the description of the electro-optical properties of CT states in organic optoelectronic devices and foster the use of organic D-A blends in energy conversion applications involving visible and ultra-violet photons [8] [9] [10] [11].

Main Text

Optical or electrical excitation at organic D-A interfaces results in the formation of CT states, where the electron almost fully resides on A and the hole on D [12]. The decay of an excited CT state regenerates a neutral ground-state, a process ideally accompanied by the emission of a photon with an energy below the optical gaps (E_{opt}) of both D and A. When employed for OLEDs [6] [13] [14], such emission from intermolecular excitations is often termed exciplex emission [2] [15] [16]. In OSCs, a similar type of intermolecular CT state has been shown to be essential for an efficient generation of free charge carriers upon illumination [17] [18]. The energy of the CT state (E_{CT}) has been demonstrated to limit the open-circuit voltage (V_{oc}) and, consequently, the overall photovoltaic PCE [19]. Typically, the difference between E_{CT} and eV_{oc} (e is the elementary charge) is about 0.2-0.3 eV higher than for inorganic and perovskite-based technologies, the reason being the dominance of non-radiative decay pathways causing additional voltage losses (ΔV_{nr}) [3] [20]. In this respect, the photovoltage of OSCs would benefit

substantially by approaching the high EQE_{EL} values as reported for the technically akin visible-light-emitting D-A blends [6]. It is therefore crucial to better understand which molecular and microstructural properties are responsible for the emissive and charge-generating nature of those organic D-A interfaces. In this work, we study archetypical D-A combinations, as reported for OLEDs and OSCs. In both cases, we detect intermolecular CT emission, but also CT absorption originating from the same manifold of intermolecular states. We demonstrate that equilibrium between CT states and free charge carriers is a necessary requirement to achieve a good photovoltaic performance, which moreover also results in low turn-on voltages for EL. For the visible-light-emitting and comparably efficient D-A blends ($\text{EQE}_{\text{EL}} > 1\%$), we observe a severe reduction of ΔV_{nr} , reaching values between 0.09-0.13 V, i.e. more than 0.15 V lower as compared to typical values (0.25-0.35 V) in the currently highest performing OSC blends [3]. We attribute these strongly reduced losses to an increased E_{CT} , effectively suppressing non-radiative decay by reducing the electron-phonon coupling. This opens up perspectives for organic materials to efficiently convert the energy of visible and UV photons, for example for applications in smart, UV-VIS absorbing windows [8], photovoltaic devices for indoor applications [9], or high-voltage multi-junction OSCs [10] [11].

We characterize the OSC performance for a typical OSC (DCV5T-Me:C₆₀ [10]) and two CT-OLEDs (BF-DPB:TmPPPyTz and BF-DPB:B4PYMPM). Due to their high E_{opt} , the photocurrent of the CT-OLEDs under solar illumination is much lower than for DCV5T-Me:C₆₀. For chemical structures and photovoltaic performance, see Figure 1a, e-g; the energy levels are listed in Supplementary Table 5. The peak value of the photovoltaic external quantum efficiency (EQE_{PV}) of the BF-DPB based devices is about 31% (B4PYMPM as A) and 18% (TmPPPyTz as A), while it is 75% for DCV5T-Me:C₆₀ (Supplementary Figure 1a, b). Fill factors (FF) of 65% and 70% are achieved for DCV5T-Me:C₆₀ and BF-DPB:B4PYMPM, while the FF for BF-DPB:TmPPPyTz is much lower (<42%). The peak of EL is at 2.14 eV for both BF-DPB based blends with an EQE_{EL} of 1.5% and 2.6% respectively, while the peak emission for DCV5T-Me:C₆₀ is about 1 eV lower with an EQE_{EL} of 0.0006%. The V_{oc} at 1 sun illumination intensity of the CT-OLEDs is very high: 2.04 V and 2.13 V, respectively, approaching the equivalent energy of the emission peak and indicating exceptionally low voltage losses for these devices. For all three devices, we sensitively measure the EQE_{PV} and EL spectra, revealing distinct low-energy absorption and emission features, below the E_{opt} the constituting neat D and A materials (Figure 1b-d). In all cases, the measured

absorption and emission spectra obey the reciprocity relation which connects both quantities [19] [21], thereby proving that both absorption and emission originate from the same electronic state, the CT state. Therefore, the term exciplex should be avoided to denote this state, since its original definition implies the absence of a stable ground state and corresponding characteristic absorption band [22] [16].

We investigate additional visible-light-emitting D-A systems of which the photovoltaic parameters are summarized in Supplementary Table 1 and EQE_{PV} and EL spectra are shown in Supplementary Figure 3. From the EL and EQE_{PV} spectra, we obtain E_{CT} and the reorganization energy by Gaussian fits, following the method outlined earlier [19]. As indicated in Figure 1b-d, E_{CT} corresponds to the intersection point of the appropriately normalized reduced EQE_{PV} and EL spectra [17].

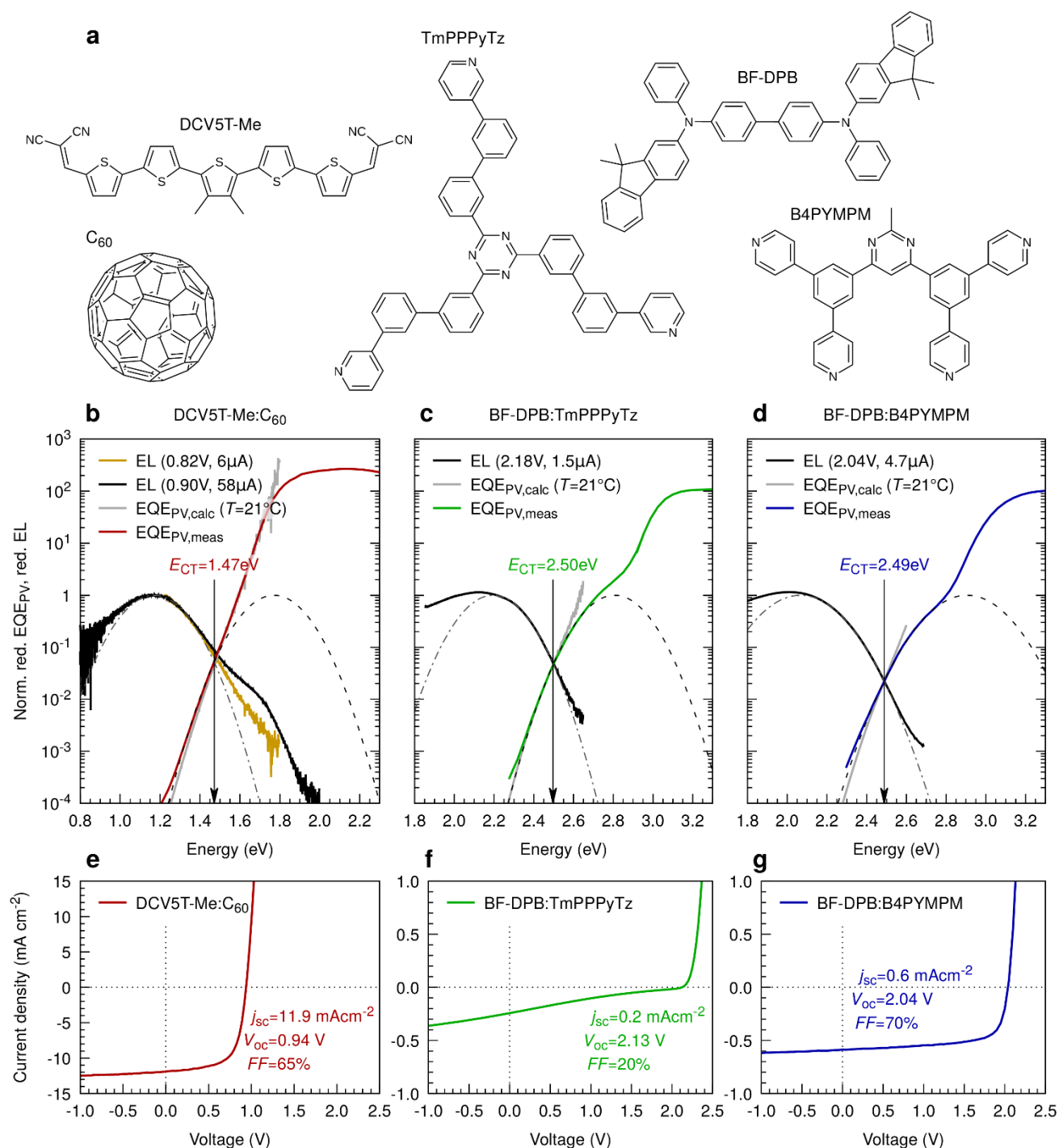


Figure 1 | Studied material systems, reciprocity relation between CT absorption and emission, and current-voltage characteristics. **a** Chemical structures of the investigated material systems. **b-d** Normalized reduced EL and EQEPV spectra as a function of the photon energy for three exemplary devices. The EL was measured using low injection currents to ensure that charge carriers reach thermal equilibrium prior to recombination. The light grey line shows an excellent agreement of the calculated EQEPV spectrum under the assumption of reciprocity between absorption and emission, and the measured EQEPV. The dashed curves show Gaussian fits to either the EL or the EQEPV spectra, following the method outlined in reference [19]. The crossing point between appropriately scaled EQEPV and EL represents E_{CT} , highlighted by a vertical black arrow. **b** Shows a well performing OSCs consisting of DCV5T-Me as D and C₆₀ as A. Here, the EL is shown for 2 different injection currents to better cover the full spectral range, where only the low-injection curve was used to analyse

the reciprocity. **c** and **d** present devices made of typical CT-OLED materials: BF-DPB:TmPPPyTz and BF-DPB:B4PYMPM, respectively **e-g** Corresponding current-density voltage curves measured under simulated AM1.5g solar illumination.

As demonstrated by the BF-DPB:B4PYMPM device, an efficient charge-carrier generation under illumination and efficient CT emission do not need to be mutually exclusive properties. Indeed, this device has a photovoltaic internal quantum efficiency (IQE_{PV}) of 83%, a FF of 70%, and an EQE_{EL} of 1.5%, see Supplementary Figure 1, 2 and Supplementary Table 1. The significantly lower IQE_{PV} and FF for the TmPPPyTz devices as compared to those containing B4PYMPM are due to more strongly bound CT states in the former, as will be shown below. We obtain deeper insights into the energetics of the CT states with respect to the energy of free charge carriers by performing temperature-dependent measurements of V_{oc} at different light intensities (Suns- V_{oc} measurements). The photo-generated current density at a specific incident illumination intensity (J_{ph}) is linked to V_{oc} and temperature (T) by the Shockley equation for open-circuit conditions [23]:

$$J_{\text{ph}} = J_{00} \exp \left[\frac{eV_{\text{oc}} - E_{\text{A,PV}}}{n_{\text{id}} k_{\text{B}} T} \right], \quad (1)$$

where $E_{\text{A,PV}}$ is the activation energy for recombination corresponding to the value of eV_{oc} extrapolated to $T=0$ K, J_{00} is the maximum theoretical recombination current, n_{id} the diode ideality factor, and k_{B} the Boltzmann constant [23]. Figure 2a-c show three exemplary temperature-dependent Suns- V_{oc} measurements for DCV5T-Me:C₆₀, BF-DPB:TmPPPyTZ, and BF-DPB:B4PYMPM (colored lines). The orange line in the side panels of Figure 2a-c correspond to $E_{\text{A,PV}}$, being the average of values determined using Eq. (1) at various illumination intensities. The fact that $E_{\text{A,PV}}$ is nearly independent of the illumination intensity proves the validity of Eq. (1). The deviations at low intensities are caused by an increased influence of the shunt resistance, which gets more pronounced at high temperatures [24]. For DCV5T-Me:C₆₀, $E_{\text{A,PV}}$ has a value of 1.39 eV which is slightly lower than its E_{CT} of 1.47 eV (see Figure 2a). In contrast, for BF-DPB:TmPPPyTz, $E_{\text{A,PV}}$ lies about 0.15 eV above E_{CT} (Figure 2b), while for BF-DPB:B4PYMPM, $E_{\text{A,PV}}$ equals E_{CT} within 0.01 eV.

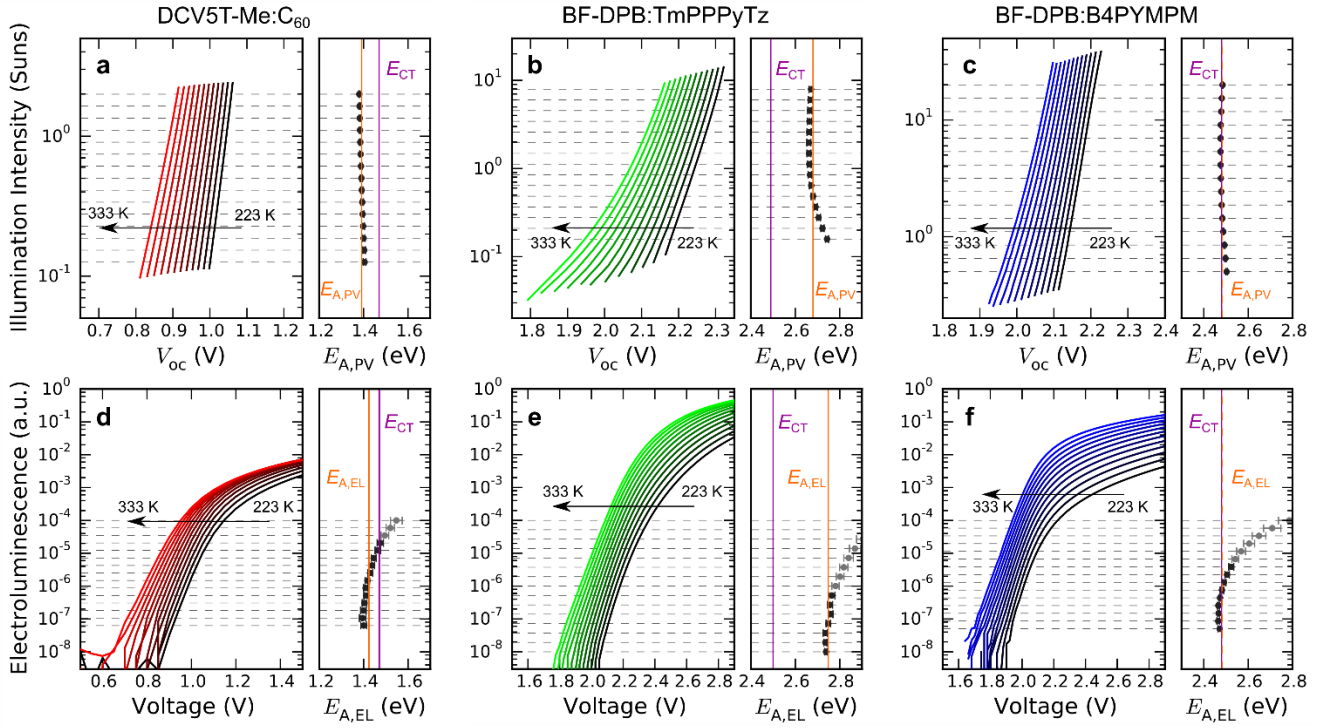


Figure 2 | Temperature-dependent V_{oc} and the EL measurements. Upper figures show temperature-dependent Suns- V_{oc} measurements of **a** DCV5T-Me:C₆₀, **b** BF-DPB:TmPPPyTz, **c** and BF-DPB:B4PYMPM. Lower figures show temperature-dependent EL measurements of **d** DCV5T-Me:C₆₀, **e** BF-DPB:TmPPPyTz, **f** and BF-DPB:B4PYMPM. In all measurements, the temperature was varied between 223 K and 333 K in steps of 10 K, as indicated by the black arrow. Grey dashed lines indicate fixed light intensities or emitted photon counts at which the voltage is taken as a function of temperature and extrapolated to 0 K. The corresponding fitted activation energies $E_{A,PV}$ and $E_{A,EL}$ are shown in the side panels as dots, with the error bar corresponding to the fitting error. For activation energies with fitting errors smaller than 15 meV the average is taken and indicated by a vertical orange line. Fits are shown in Supplementary Figure 5. The optically determined E_{CT} is plotted as a purple vertical line.

The activation energy $E_{A,EL}$ of the emitted light intensity behaves similarly as $E_{A,PV}$, resulting in an equation analogous to equation (1) for the emitted photon flux ϕ at low injection currents [12]:

$$\phi = \phi_{00} \exp \left[\frac{eV - E_{A,EL}}{k_B T} \right], \quad (2)$$

with ϕ_{00} as the maximum theoretical photon flux. Photon-flux vs. voltage measurements at different temperatures as well as the extracted $E_{A,EL}$ values are shown in Figure 2d-f. Note that $E_{A,PV}$ and $E_{A,EL}$ are equal to each other within 0.07 eV for small injection currents. Therefore, in the remainder of the text we denote $E_A \approx E_{A,PV} \approx E_{A,EL}$. All values are summarized in Supplementary Table 1, including further D materials in combination with TmPPPyTz and B4PYMPM, whose temperature-dependent analysis is shown in Supplementary Figure 4, 6. In general, we find the following correlation: high FF devices

exhibit E_A smaller or equal to E_{CT} , while for poor FF devices E_A is significantly larger than E_{CT} . In what follows, we will rationalize this observation and will show that $E_A - E_{CT}$ is a good measure for the CT state binding energy. Consider therefore the electronic processes regulating the conversion of CT states at energy E_{CT} into free charge carriers at energy E_{FC} and vice versa.

In the case that the CT state is strongly bound, every free electron-hole encounter will result in CT state decay, independent of the value of E_{CT} . One can derive that in that case $E_A = E_{FC}$, making $E_A - E_{CT}$ equal to the CT state binding energy [12]. When TmPPPyTz is used as acceptor, $E_A - E_{CT}$ is larger than a few $k_B T$ and the FF and IQE_{PV} are indeed significantly reduced (see Supplementary Table 1), since in this case CT state (re-)dissociation is a very rare process. Accordingly, the lifetime of the CT state is determined by the CT state decay rate only, while the lifetime of the free carriers is determined by their encounter rate. Often, these assumptions are made implicitly for OLEDs, but as shown below, they are not correct for the B4PYMPM containing devices studied [25].

If CT state dissociation occurs much faster than CT state decay, free carriers and CT states are transformed into each other several times before CT state decay. One can derive that $E_A = E_{CT}$ [12] and the populations of free carriers and CT states decay at the same overall rate. Such an equilibrium of CT states and free carriers before decay is a prerequisite for efficient photocurrent generation and high FF s. This is consistent with the fact that devices containing C_{60} and B4PYMPM as acceptor have good photovoltaic characteristics (Figure 1e and g) and E_A is not substantially higher than E_{CT} . Furthermore, as the onset voltages for EL emission are in this case determined by E_{CT} instead of E_{FC} , they can be substantially reduced. Indeed the onset for EL emission occurs for BF-DPB:B4PYMPM ($E_A \approx E_{CT}$) at about 0.2 eV lower than for BF-DPB:TmPPPyTz ($E_A - E_{CT} \approx 0.2$ eV), even though E_{CT} is rather similar in these systems (Figure 2e and f).

The beneficial properties of B4PYMPM with respect to free carrier photo-generation and associated low onset voltage for emission are likely associated with the ability of B4PYMPM to form molecular stacks with a rather high charge carrier mobility, providing pathways for CT states to dissociate [26]. Indeed, when using B3PYMPM, a very similar molecule as compared to B4PYMPM but with much less tendency

to stack [26], we find a significant CT state binding energy, as well as a reduced photovoltaic performance and a substantially lower FF (see Supplementary Figure 7 and 8).

The visible light emitting devices studied in this work have a 1,000 to 10,000 times higher EQE_{EL} than typical OSC blends [3] [27], irrespective of their charge generating properties and CT state binding energy. This results in about 0.20 V reduction of the non-radiative voltage losses (ΔV_{nr}) which are related to the EQE_{EL} by [3]:

$$\Delta V_{nr} = \frac{k_B T}{e} \ln \left(\frac{1}{EQE_{EL}} \right). \quad (3)$$

In the concrete example of BF-DPB:TmPPPyTz and BF-DPB:B4PYMPM, ΔV_{nr} is 0.09 V and 0.10 V, resulting in $E_{CT}-eV_{oc}$ differences of 0.37 eV and 0.45 eV respectively. For the DCV5T-Me:C₆₀, a significantly higher ΔV_{nr} of 0.29 V and $E_{CT}-eV_{oc}$ of 0.53 eV are found, being typical for current state-of-the-art OSCs [3] [28] [4]. Figure 3 plots V_{oc} , ΔV_{nr} and EQE_{EL} as a function of E_{CT} . Previously published data on fullerene containing OSCs [3] are supplemented by data for vacuum and solution processed devices based on non-fullerene acceptors (NFAs), including the high- E_{CT} devices discussed above. Also with the addition of these new devices, a trend where ΔV_{nr} decreases with increasing E_{CT} can be observed. This prevailing trend therefore indicates that non-radiative decay in fullerene and non-fullerene based D-A devices is intrinsically linked to electron-phonon coupling [3]. These findings are in accordance with the energy-gap law, which describes that in organic molecules the non-radiative decay rate is exponentially decreasing with the energy difference between electronically excited state and ground state [3] [29]. The devices discussed above extend the analysis to E_{CT} values in the visible region of the electromagnetic spectrum. Only for these high E_{CT} devices, we find significantly reduced voltage losses and EQE_{EL} values of about 1%, bringing them closer to their theoretical maximum V_{oc} as given by the Shockley-Queisser limit (Figure 3a). For the set of data plotted in Figure 3b, a small deviation from the approximately linear relation of $\Delta V_{nr} \propto E_{CT}$ can be observed. These are likely caused by a variation of the molecular parameters influencing the energy-gap law [30]. Nevertheless, the impressive span of the trend between ΔV_{nr} and E_{CT} for a large energy range indicates that the main figure of merit substantially altering the non-radiative decay is plainly found in the value of E_{CT} . Details of the chemical structures of D and A are of secondary importance, as we find for both fullerene and NFA containing OSCs non-radiative voltage losses within the same range for a given E_{CT} .

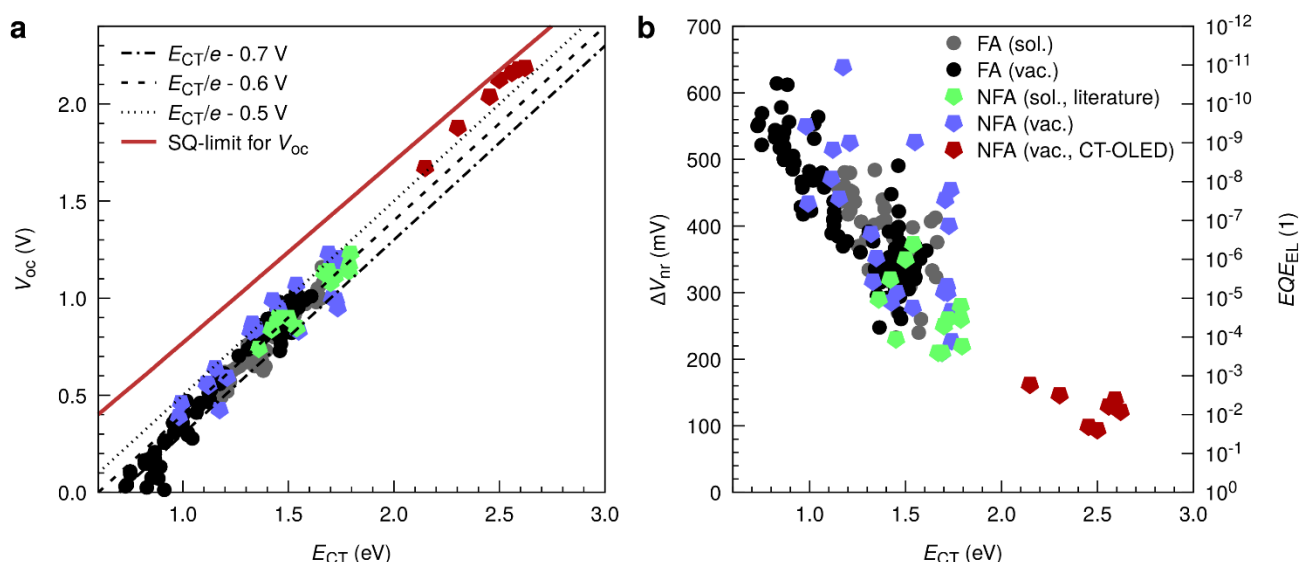


Figure 3 | Open-circuit voltage and non-radiative voltage losses as function of E_{CT} . **a** V_{OC} and **b** ΔV_{nr} as a function of E_{CT} for more than 170 different OSCs which are based on fullerene (FA) (circles) or NFAs (pentagons). Devices processed from solution are represented by grey and green symbols, all the others are processed by evaporation. The data shown by grey, light-green and black symbols were published previously [27] [3] [31] [32] [4] [28] [33] [34] [35]. CT-OLED devices discussed in this publication are shown in red. Details on all devices can be found in Supplementary Table 3.

We conclude this work by pointing out that we have found visible-light-emitting D-A systems with voltage losses $E_{CT}-eV_{OC}$ as low as 0.37 eV. This value is severely reduced as compared to the typical values of 0.60 eV for OSCs, and approaches the voltage losses of GaAs of 0.32 eV [36]. This is the direct consequence of decreasing non-radiative decay pathways, resulting in EQE_{EL} values in the percent range. However, in the particular case of the BF-DPB:TmPPPyTz blend, temperature-dependent measurements show that the CT state has a binding energy of about 0.15-0.20 eV, resulting in a reduced FF and IQE_{PV} . In contrast, we demonstrate that for a BF-DPB:B4PYMPM blend with a similar CT state energy of 2.49 eV, the CT emission quantum yield is 1000-10000 times higher than for typical OSC materials, while the FF of 70% and IQE_{PV} of 83% are comparable to well performing OSCs. This work therefore shows that efficient photogeneration of free carriers and a high electroluminescence quantum yield do not necessarily need to be mutually exclusive in organic semiconductors. The resulting reduced non-radiative voltage losses, on par of or even below those of inorganic technologies, make visible-light-emitting D-A systems interesting for an efficient capture and low-energy-loss conversion of visible photons in photovoltaics, for example for indoor application and multi-junction solar cells.

Methods

Device preparation: The layers of the OSCs are thermally evaporated at ultra-high vacuum (base pressure $< 10^{-7}$ mbar) on a glass substrate with a pre-structured ITO contact (Thin Film Devices, USA). Glass substrates are cleaned in a multi-step wet process including rinsing with N-methyl-2-pyrrolidone, ethanol, and deionized water as well as treatment with ultraviolet ozone. Details on the layer sequence for each device are listed in Supplementary Table 2. We tested different hole transport layer for the high-gap devices, the results are listed in Supplementary Table 4. All organic materials were purified 2-3 times by sublimation. The device area is defined by the geometrical overlap of the bottom and the top contact and equals 6.44 mm^2 . To avoid exposure to ambient conditions, the organic part of the device was covered by a small glass substrate, which is glued on top.

Current-voltage characteristics in dark and under solar illumination are measured with a SMU (Keithley 2400, USA) at room temperature in ambient conditions. The cells are illuminated with a spectrally mismatch corrected intensity of 100 mW cm^{-2} (AM1.5g) provided by a sun simulator (16 S-150 V.3 Solar Light Co., USA). Masks are used to minimize edge effects and to define an exact photoactive area (2.78 mm^2). The intensity is monitored with a Hamamatsu S1337 silicon photodiode (calibrated by Fraunhofer ISE Freiburg, Germany). Light-intensity-dependent *FF* measurement of the CT-OLEDs were conducted by using three 385 nm APG2C1-385-r2 UV LEDs (Roithner, Austria) in series as illumination source and a Keithley SMU 2635A to measure the current-voltage curve.

EQE_{PV} measurements: have been performed according to previous works and reproduced here for completeness [3] [10]. EQE_{PV} is measured using masks to minimize edge effects and to define an exact photoactive area (2.78 mm^2). The EQE_{PV} is detected with a lock-in amplifier (Signal Recovery SR 7265) under monochromatic illumination (Oriel Xe Arc-Lamp Apex Illuminator combined with Cornerstone 260 1/4m monochromator, Newport, USA) using a calibrated mono-crystalline silicon reference diode (Hamamatsu S1337 calibrated by Fraunhofer ISE, Germany). For sensitively measured EQE_{PV} the light of a quartz halogen lamp (50 W), used for the low- E_{CT} devices, or a white high-power LED (LED Engin LZP-00CW00, USA), used for the high- E_{CT} devices, is chopped at 140 Hz and coupled into a

monochromator (Newport Cornerstone 260 1/4m, USA). The resulting monochromatic light is focused onto the OSC, its current at short-circuit conditions is fed to a current pre-amplifier before it is analysed with a lock-in amplifier (Signal Recovery 7280 DSP, USA). The time constant of the lock-in amplifier was chosen to be 1s and the amplification of the pre-amplifier was increased to resolve low photocurrents. The EQE_{PV} is determined by dividing the photocurrent of the OSC by the flux of incoming photons, which was measured using a calibrated Si and InGaAs photodiode (FDS100-CAL and FGA21-CAL, Thorlabs Inc., USA).

Electroluminescence measurements have been performed according to previous work and reproduced here for completeness [37]. The EL spectra were obtained with an Andor SR393i-B spectrometer equipped with a cooled Si and cooled InGaAs CCD detector array (DU420A-BR-DD and DU491A-1.7, UK). The spectral response of the setup was calibrated with a reference lamp (Oriel 63355). The emission spectrum of the OSCs was recorded at different injection currents with respect to voltages, which were lower than or at least similar to the V_{oc} of the device at 1 sun illumination. Additional certification of the EL measurements was determined by a flux calibrated Acton SpectraPro SP2560 monochromator coupled to a cooled Spec10LN Si CCD camera from Princeton Instruments.

EQE_{EL} measurements have been performed according to previous work and reproduced here for completeness [3]. The EQE_{EL} was measured by forward biasing the OSCs with either an Agilent 4155C parameter analyser or Keithley SMU and collecting the emitted radiation by an enhanced G10899-03K InGaAs photodetector from Hamamatsu. The absolute total photon flux determination was performed by placing the OSC at a distance of 18.3 mm from the photodetector. Knowledge about the spectral distribution of the cell emission, the spectral response of the InGaAs photodetector, and the assumption of a point source emitting uniformly into a half-sphere allows for the determination of the absolute EL photon flux from the OSC. Uncertainties in measured EQE_{EL} are expected to be governed by the small distance imprecision between the OSC and the photodetector (calibrated Si detector from Newport, 818-series with an active area of 1 cm²). To keep this uncertainty as little as possible, the measurement is conducted in different distances from the solar cell and always extrapolated to the full half sphere.

Temperature dependent Suns- V_{oc} and EL measurements have been conducted with a self-made set-up. For Suns- V_{oc} measurements, a Keithley SMU2635A is controlling the LED (a white LED (APG2C3-NW, Roithner, Austria) for the OSCs and a 365 nm LED (APG2C1-365-r4, Roithner) for the CT-OLEDs) to change the light intensity. A Keithley dual channel SMU2602A measures both the V_{oc} and the illumination intensity with a Newport 818-UV photodiode. To measure the EL, the dual channel SMU2602A applies a bias voltage to the sample, and measures the photocurrent of a S2387-66R Si Photodiode (Hamamatsu, Japan), which is directly attached to the device, covering the whole active area. To change the cell temperature, the devices are placed in vacuum on a copper block, which is connected to a Peltier element from Peltron GmbH (Fürth, Germany), controlled by a BelektroniG HAT Control device (Freital, Germany). The measurement equipment is controlled with the software SweepMe! (obtained from: <https://sweep-me.net>).

Determination of the IQE_{PV} : The IQE_{PV} of the investigated devices was obtained by dividing the experimental EQE_{PV} with the simulated absorption of the active layer of each device. Optical simulations were performed using a numerical code based on the transfer matrix method which uses the refractive index n , extinction coefficient k , and the layer thickness to calculate photon absorption and the distribution of the optical field within the solar cell. Variable angle spectroscopic ellipsometry (VASE) has been performed in order to determine the n and k values of the active layers (BF-DPB:TmPPPyTz and BF-DPB:B4PYMPM) utilizing an EP4 imaging ellipsometer (accurion GmbH, Germany). The ellipsometric parameters Ψ and Δ of 50 nm thick layers on quartz glass substrates have been measured for two different angles of incidence (50°, 60°) in a wavelength range from 360 nm to 700 nm and were approximated with an isotropic model containing two Gaussian oscillators.

Data Availability Statement

The data that support the plots within this paper and other findings of this study are available from the corresponding authors S.U., J.B., and K.V. upon reasonable request.

Corresponding Authors

Correspondence and request for materials should be addressed to S.U., J.B., or K.V.

Acknowledgements

This work was supported by the German Federal Ministry for Education and Research (BMBF) through the InnoProfile project “Organische p-i-n Bauelemente 2.2” (03IPT602X) and by the German Research Foundation (DFG) project Photogen (VA 1035/5-1). X.J. and Y.L. acknowledge the China Scholarship Council (No. 201706140127 and No. 201506920047, respectively). Moreover, we acknowledge the DFG for supporting K.T. (project 382633022 “RECOLPER”), F.P., S.Ro., and D.N. (SFB 951 “HIOS”), and A.F. (RE 3198/6-1 “EFOD”).

Author Contribution

S.U., J.B., X.J., D.S., and K.V. designed the experiments, prepared photovoltaic devices and optimized their processing parameters for photovoltaic performance. S.U., X.J., Y.L., and J.W. performed the temperature-dependent characterization of the devices. J.B. and X.J. measured the sensitive EQE_{PV} spectra, K.T., V.C.N., F.P., S.Ro. measured the EQE_{EL} and the corresponding EL spectra. D.N., A.F., S.Re., and K.V. supervised sub-tasks (OPV and OLED design, investigation, and data interpretation) within the project and participated in discussion of the findings. K.V. supervised the overall project. All authors contributed to the data analysis and writing of the manuscript.

Competing Financial Interests

The authors declare no competing financial interests.

- [1] C. Yan, S. Barlow, Z. Wang, H. Yan, A. K.-Y. Jen, S. R. Marder and X. Zhan, “Non-fullerene acceptors for organic solar cells,” *Nat. Rev. Mater.*, vol. 3, p. 18003, 2018.
- [2] M. Sarma and K.-T. Wong, “Exciplex: An Intermolecular Charge-Transfer Approach for TADF,” *ACS Appl. Mater. Interfaces*, vol. 10, p. 19279–19304, 2018.
- [3] J. Benduhn, K. Tvingstedt, F. Piersimoni, S. Ullbrich, Y. Fan, M. Tropiano, K. A. McGarry, O. Zeika, M. K. Riede, C. J. Douglas, S. Barlow, S. R. Marder, D. Neher, D. Spoltore and K. Vandewal, “Intrinsic non-radiative voltage losses in fullerene-based organic solar cells,” *Nat. Energy*, vol. 2, p. 17053, 2017.
- [4] D. Qian, Z. Zheng, H. Yao, W. Tress, T. R. Hopper, S. Chen, S. Li, J. Liu, S. Chen, J. Zhang, X. K. Liu, B. Gao, L. Ouyang, Y. Jin, G. Pozina, I. A. Buyanova, W. M. Chen, O. Inganäs, V. Coropceanu, J. L. Bredas, H. Yan, J. Hou, F. Zhang, A. A. Bakulin and F. Gao, “Design rules for minimizing voltage losses in high-efficiency organic solar cells,” *Nat. Mater.*, vol. 17, no. 8, pp. 703-709, 2018.
- [5] K. Goushi, K. Yoshida, K. Sato and C. Adachi, “Organic light-emitting diodes employing efficient reverse intersystem crossing for triplet-to-singlet state conversion,” *Nat. Photon.*, vol. 6, no. 4, pp. 253-258, 2012.
- [6] D. Chen, G. Xie, X. Cai, M. Liu, Y. Cao and S. J. Su, “Fluorescent Organic Planar pn Heterojunction Light-Emitting Diodes with Simplified Structure, Extremely Low Driving Voltage, and High Efficiency,” *Adv. Mater.*, vol. 28, pp. 239-244, 2016.
- [7] T.-C. Lin, M. Sarma, Y.-T. Chen, S.-H. Liu, K.-T. Lin, P.-Y. Chiang, W.-T. Chuang, Y.-C. Liu, H.-F. Hsu, W.-Y. Hung, W.-C. Tang, K.-T. Wong and P.-T. Chou, “Probe exciplex structure of highly efficient thermally activated delayed fluorescence organic light emitting diodes,” *Nat. Comm.*, vol. 9, no. 1, p. 3111, 2018.
- [8] N. C. Davy, M. Sezen-Edmonds, J. Gao, X. Lin, A. Liu, N. Yao, A. Kahn and Y.-L. Loo, “Pairing of near-ultraviolet solar cells with electrochromic windows for smart management of the solar spectrum,” *Nat. Energy*, vol. 2, p. 17104, jun 2017.
- [9] C. Lungenschmied, G. Dennler, H. Neugebauer, S. N. Sariciftci, M. Glatthaar, T. Meyer and A. Meyer, “Flexible, long-lived, large-area, organic solar cells,” *Sol. Energ. Mater. Sol. C.*, vol. 91, no. 5, pp. 379-384, 2007.
- [10] R. Meerheim, C. Körner and K. Leo, “Highly efficient organic multi-junction solar cells with a thiophene based donor material,” *Appl. Phys. Lett.*, vol. 105, p. 063306, 2014.
- [11] L. Meng, Y. Zhang, X. Wan, C. Li, X. Zhang, Y. Wang, X. Ke, Z. Xiao, L. Ding, R. Xia, H.-I. Yip, Y. Cao and Y. Chen, “Organic and solution-processed tandem solar cells with 17.3% efficiency,” *Science*, vol. 6407, pp. 1094-1098, 2018.
- [12] K. Vandewal, “Interfacial Charge Transfer States in Condensed Phase Systems,” *Annu. Rev. Phys. Chem.*, vol. 67, pp. 113-133, 2016.
- [13] X. K. Liu, Z. Chen, C. J. Zheng, C. L. Liu, C. S. Lee, F. Li, X. M. Ou and X. H. Zhang, “Prediction and design of efficient exciplex emitters for high-efficiency, thermally activated delayed-fluorescence organic light-emitting diodes,” *Adv. Mater.*, vol. 27, pp. 2378-2383, 2015.
- [14] W. Chang, D. N. Congreve, E. Hontz, M. E. Bahlke, D. P. McMahon, S. Reineke, T. C. Wu, V. Bulovic, T. V. Voorhis and M. A. Baldo, “Spin-dependent charge transfer state design rules in organic photovoltaics,” *Nature Communications*, vol. 6, p. 6415, 2015.

- [15] A. a. H. A. Attar and A. P. Monkman, "Electric Field Induce Blue Shift and Intensity Enhancement in 2D Exciplex Organic Light Emitting Diodes; Controlling Electron–Hole Separation," *Adv. Mater.*, vol. 28, pp. 8014-8020, 2016.
- [16] S. A. Jenekhe and J. A. Osaheni, "Excimers and exciplexes of conjugated polymers," *Science*, vol. 265, pp. 765-768, 1994.
- [17] K. Vandewal, S. Albrecht, E. T. Hoke, K. R. Graham, J. Widmer, J. D. Douglas, M. Schubert, W. R. Mateker, J. T. Bloking, G. F. Burkhard, A. Sellinger, J. M. J. Fréchet, A. Amassian, M. K. Riede, M. D. McGehee, D. Neher and A. Salleo, "Efficient charge generation by relaxed charge-transfer states at organic interfaces," *Nat. Mater.*, vol. 13, no. 1, pp. 63-68, 2014.
- [18] S. H. Park, A. Roy, S. Beaupre, S. Cho, N. Coates, J. S. Moon, D. Moses, M. Leclerc, K. Lee and A. J. Heeger, "Bulk heterojunction solar cells with internal quantum efficiency approaching 100%," *Nat. Photon.*, vol. 3, no. 5, pp. 297-303, 2009.
- [19] K. Vandewal, K. Tvingstedt, A. Gadisa, O. Inganäs and J. V. Manca, "Relating the open-circuit voltage to interface molecular properties of donor:acceptor bulk heterojunction solar cells," *Phys. Rev. B*, vol. 81, no. 12, p. 125204, 2010.
- [20] K. Tvingstedt, O. Malinkiewicz, A. Baumann, C. Deibel, H. J. Snaith, V. Dyakonov and H. J. Bolink, "Radiative efficiency of lead iodide based perovskite solar cells," *Nat. Scientific Reports*, vol. 4, p. 6071, 2014.
- [21] U. Rau, "Reciprocity relation between photovoltaic quantum efficiency and electroluminescent emission of solar cells," *Phys. Rev. B*, vol. 76, p. 085303, 2007.
- [22] A. D. McNaught and A. Wilkinson, IUPAC. Compendium of Chemical Terminology, 2nd ed. (t ed., Oxford, UK: Blackwell Scientific Publications, 1997.
- [23] K. Tvingstedt and C. Deibel, "Temperature Dependence of Ideality Factors in Organic Solar Cells and the Relation to Radiative Efficiency," *Adv. Energy Mater.*, vol. 6, no. 9, p. 1502230, 2016.
- [24] S. Banerjee and W. A. Anderson, "Temperature dependence of shunt resistance in photovoltaic devices," *Appl. Phys. Lett.*, vol. 49, pp. 38-40, 1986.
- [25] D. a. P. L. Santos, F. B. Dias and A. P. Monkman, "Investigation of the Mechanisms Giving Rise to TADF in Exciplex States," *J. Phys. Chem. C*, vol. 120, pp. 18259-18267, 2016.
- [26] D. Yokoyama, H. Sasabe, Y. Furukawa, C. Adachi and J. Kido, "Molecular stacking induced by intermolecular C-H...N hydrogen bonds leading to high carrier mobility in vacuum-deposited organic films," *Adv. Funct. Mater.*, vol. 21, pp. 1375-1382, 2011.
- [27] J. Liu, S. Chen, D. Qian, B. Gautam, G. Yang, J. Zhao, J. Bergqvist, F. Zhang, W. Ma, H. Ade, O. Inganäs, K. Gundogdu, F. Gao and H. Yan, "Fast charge separation in a non-fullerene organic solar cell with a small driving force," *Nat. Energy*, vol. 1, no. 9, p. 16089, 2016.
- [28] X. Liu, X. Du, J. Wang, C. Duan, X. Tang, T. Heumueller, G. Liu, Y. Li, Z. Wang, J. Wang, F. Liu, N. Li, C. J. Brabec, F. Huang and Y. Cao, "Efficient Organic Solar Cells with Extremely High Open-Circuit Voltages and Low Voltage Losses by Suppressing Nonradiative Recombination Losses," *Adv. Energy Mater.*, p. 1801699, 2018.
- [29] R. Englman and J. Jortner, "The energy gap law for radiationless transitions in large molecules," *Mol. Phys.*, vol. 18, no. 2, pp. 145-164, 1970.

- [30] M. Azzouzi, J. Yan, T. Kirchartz, K. Liu, J. Wang, H. Wu and J. Nelson, “Nonradiative Energy Losses in Bulk-Heterojunction Organic Photovoltaics,” *Phys. Rev. X*, vol. 8, no. 3, p. 31055, 2018.
- [31] D. Yang, Y. Wang, T. Sano, F. Gao, H. Sasabe and J. Kido, “A minimal non-radiative recombination loss for efficient non-fullerene all-small-molecule organic solar cells with a low energy loss of 0.54 eV and high open-circuit voltage of 1.15 V,” *J. Mater. Chem. A*, pp. 13918-13924, 2018.
- [32] Z. Tang, B. Liu, A. Melianas, J. Bergqvist, W. Tress, Q. Bao, D. Qian, O. Inganäs and F. Zhang, “A New Fullerene-Free Bulk-Heterojunction System for Efficient High-Voltage and High-Fill Factor Solution-Processed Organic Photovoltaics,” *Adv. Mater.*, vol. 27, no. 11, pp. 1900-1907, 2015.
- [33] V. C. Nikolis, J. Benduhn, F. Holzmueller, F. Piersimoni, M. Lau, O. Zeika, D. Neher, C. Koerner, D. Spoltore and K. Vandewal, “Reducing Voltage Losses in Cascade Organic Solar Cells while Maintaining High External Quantum Efficiencies,” *Adv. Energy Mater.*, vol. 7, no. 21, p. 1700855, 2017.
- [34] W. Zhao, D. Qian, S. Zhang, S. Li, O. Inganäs, F. Gao and J. Hou, “Fullerene-free polymer solar cells with over 11% efficiency,” *Adv. Mater.*, vol. 28, pp. 4734-4739, 2016.
- [35] J. Zhang, B. Kan, A. J. Pearson, A. J. Parnell, J. Cooper, X.-K. Liu, P. Conaghan, T. Hopper, Y. Wu, X. Wan, F. Gao, N. C. Greenham, A. A. Bakulin, Y. Chen and R. H. Friend, “Efficient Non-fullerene Organic Solar Cells Employing Sequentially Deposited Donor-Acceptor Layers,” *J. Mater. Chem. A*, vol. 6, pp. 18225-18233, 2018.
- [36] B. M. Kayes, H. Nie, R. Twist, S. G. Spruytte, F. Reinhardt, I. C. Kizilyalli and G. S. Higashi, “27.6% Conversion efficiency, a new record for single-junction solar cells under 1 sun illumination,” in *IEEE Photovoltaic Specialists Conference*, 2011.
- [37] J. Benduhn, F. Piersimoni, G. Londi, A. Kirch, J. Widmer, C. Koerner, D. Beljonne, D. Neher, D. Spoltore and K. Vandewal, “Impact of Triplet Excited States on the Open-Circuit Voltage of Organic Solar Cells,” *Adv. Energy Mater.*, vol. 8, no. 21, p. 1800451, 2018.